

# REPORT DOCUMENTATION PAGE

*Form Approved*  
*OMB No. 0704-0188*

Public reporting burden for this collection of information is estimated to average 1 hour per response, including the time for reviewing instructions, searching existing data sources, gathering and maintaining the data needed, and completing and reviewing this collection of information. Send comments regarding this burden estimate or any other aspect of this collection of information, including suggestions for reducing this burden to Department of Defense, Washington Headquarters Services, Directorate for Information Operations and Reports (0704-0188), 1215 Jefferson Davis Highway, Suite 1204, Arlington, VA 22202-4302. Respondents should be aware that notwithstanding any other provision of law, no person shall be subject to any penalty for failing to comply with a collection of information if it does not display a currently valid OMB control number. **PLEASE DO NOT RETURN YOUR FORM TO THE ABOVE ADDRESS.**

<b>1. REPORT DATE (DD-MM-YYYY)</b> 21-06-2010		<b>2. REPORT TYPE</b> Final Report		<b>3. DATES COVERED (From - To)</b> 01-04-06 to 31-01-2010	
<b>4. TITLE AND SUBTITLE</b> Thermal Protection / Light Weight Materials Development for Future Air Force Vehicles				<b>5a. CONTRACT NUMBER</b> FA9550-06-1-0118	
				<b>5b. GRANT NUMBER</b>	
				<b>5c. PROGRAM ELEMENT NUMBER</b>	
<b>6. AUTHOR(S)</b>  Terry Creasy, J.N.Reddy				<b>5d. PROJECT NUMBER</b>	
				<b>5e. TASK NUMBER</b>	
				<b>5f. WORK UNIT NUMBER</b>	
<b>7. PERFORMING ORGANIZATION NAME(S) AND ADDRESS(ES)</b>  Texas Engineering Experiment Station      332 Wisenbaker Engineering Research Center, Texas A&M University, College Station, TX 77843-3000				<b>8. PERFORMING ORGANIZATION REPORT NUMBER</b>	
<b>9. SPONSORING / MONITORING AGENCY NAME(S) AND ADDRESS(ES)</b> Dr. Les Lee      Air Force office of Scientific Research, Program Manager for Mechanics of Materials and Devices      875 N. Randolph Street, AFOSR/NA, Suite 325, Room 3112 Arlington, VA 22203 Phone: (703)-696-8483				<b>10. SPONSOR/MONITOR'S ACRONYM(S)</b>	
				<b>11. SPONSOR/MONITOR'S REPORT NUMBER(S)</b>  AFRL-OSR-VA-TR-2012-0431	
<b>12. DISTRIBUTION / AVAILABILITY STATEMENT</b>  Distribution A: Approved for Public Release					
<b>13. SUPPLEMENTARY NOTES</b>					
<b>14. ABSTRACT</b> The overall goals of this program are to develop fast thermal dissipation mechanisms for light weight polymer matrix fibrous composites based on moisture evaporative cooling, superconducting heat pipe arrays and thermal ceramic protective coatings for future Air Force vehicles, and associated propulsion systems. In the first year of the program the following technical areas were pursued and their progress is reported on <ul style="list-style-type: none"> <li>(i) Moisture diffusion modeling and experimental liquid water capillary flow evaporative cooling together with water soluble chemicals that limit surface emission IR signatures.</li> <li>(ii) Ultrafast heat pipes as integrated structural members.</li> </ul>					
<b>15. SUBJECT TERMS</b>					
<b>16. SECURITY CLASSIFICATION OF:</b>			<b>17. LIMITATION OF ABSTRACT</b>  None	<b>18. NUMBER OF PAGES</b>  10	<b>19a. NAME OF RESPONSIBLE PERSON</b> Terry S. Creasy
<b>a. REPORT</b> Unclassified	<b>b. ABSTRACT</b> Unclassified	<b>c. THIS PAGE</b> Unclassified			<b>19b. TELEPHONE NUMBER (include area code)</b> 979-845-0118

# **FINAL REPORT**

## **Thermal Protection / Light Weight Materials Development for Future Air Force Vehicles**

### **PRINCIPAL INVESTIGATORS**

Terry Creasy

J.N. Reddy

Texas A&M University

JUNE 2010

AFOSR CONTRACT NO.:  
FA9550-06-1-0118

## **EXECUTIVE SUMMARY**

The overall goals of this program were to develop fast thermal dissipation mechanisms for lightweight polymer matrix fibrous composites based on moisture evaporative cooling, superconducting heat pipe arrays, and thermal ceramic protective coatings for future Air Force vehicles, and associated propulsion systems. The project had these outcomes:

- Models show that
  - Moisture bearing composites can delay and decrease the surface temperature rise that occurs when exposed to 90 °C; however, the effect is limited by the moisture carried by the composite and the time taken to replenish moisture in the structure.
  - Flowing evaporative cooling has a similar effect; the moisture flows through the structure to cool the surface. The method is effective for low relative humidity environments.
  
- Our experiments failed to produce components with naked internal channels for fluid circulation. This outcome suggests that channels might be made from microtubes that—when combined with the reinforcing fibers—remain in the composite to direct fluids through the structure.
  
- The superconducting heat pipes that the proposal was based upon remain controversial. To date, publications are few and show inconsistent behavior. The proposed work was to consider the superconducting heat pipes as candidates for miniaturization—assuming the superconducting properties were functional at the microscale. Data to support this plan is unavailable at this time.

# CONTENTS

<b>OBJECTIVES .....</b>	<b>5</b>
<b>STATUS OF EFFORT .....</b>	<b>6</b>
MODELS .....	6
<i>Numerical Evaluation of Active Evaporation Cooling of a Composite Panel Using the Finite Element Method .....</i>	<i>6</i>
Introduction .....	6
Physical Model .....	6
Derivation of Governing Heat Equation.....	7
Rule of Mixtures and Constitutive Relationships.....	8
Finite Element Model of Energy Equation.....	9
Weak Form of Energy Equation .....	9
Semi-Discrete Finite Element Equations.....	10
Fully Discretized Finite Element Equations.....	11
Initial and Boundary Conditions .....	11
Numerical Results and Discussion.....	12
Conclusions.....	15
MICROCHANNEL MODEL EXPERIMENTS.....	17
<i>Sample preparation .....</i>	<i>17</i>
<i>Complex microchannel.....</i>	<i>19</i>
<i>Mathematical modeling of conductive heat transfer in composites.....</i>	<i>19</i>
<i>Reference .....</i>	<i>20</i>
<b>PERSONNEL SUPPORTED/ASSOCIATED .....</b>	<b>21</b>
<b>PUBLICATIONS.....</b>	<b>22</b>
<b>APPENDIX.....</b>	<b>23</b>
A.    CONVECTIVE HEAT TRANSFER COEFFICIENTS .....	23
B.    CONVECTIVE MASS TRANSFER COEFFICIENTS .....	24
C.    MATERIAL PROPERTIES .....	24
<b>REFERENCES .....</b>	<b>26</b>

## **OBJECTIVES**

- The overall goals of this program are to develop fast thermal dissipation mechanisms for lightweight polymer matrix fibrous composites based on moisture evaporative cooling, superconducting heat pipe arrays, and thermal ceramic protective coatings for future Air Force vehicles, and associated propulsion systems. The thermal ceramic protective coating work stopped in early 2008 when the project was refocused after the tragic loss of the originating P.I., Dr. Roger J. Morgan.
- Evaporative moisture rapid surface cooling of composites will be evaluated by:-
  - Experimental diffusion of moisture from high moisture bearing fillers embedded in a polymer matrix, in conjunction with moisture diffusion modeling studies
  - A network of microcapillaries that supply water to the surface structure from an internal reservoir.
- An array of ultra-fast conducting heat pipes will be developed, that are based on internal thermal gaseous increases, which rapidly conduct surface heat to an internal heat sink.

## STATUS OF EFFORT

The project stopped technical progress in December 2009 with some report activity continuing into January 2010.

### MODELS

#### **Numerical Evaluation of Active Evaporation Cooling of a Composite Panel Using the Finite Element Method**

##### Introduction

Limiting the external temperature of stealth aircraft has become a major concern as aircraft have become more vulnerable to detection due to recent improvements in the IR signature detection devices of missile systems. If an aircraft deviates from its surroundings by only 1°C, detection can be achieved at military useful ranges [1]. Current stealth aircraft utilize cooling pipes within the wings and engine exhaust to limit external temperatures and thereby the associated IR signatures. However, more efficient and instantaneous cooling mechanisms are needed.

We numerically evaluate the potential of evaporative cooling of water as an alternative mechanism for the cooling of stealth aircraft. Evaporative cooling of liquid water occurs when the surface of a body of water or moist object is exposed to an open environment. Under these conditions, the water will begin to evaporate. This is due to the natural tendency of liquid water to achieve phase equilibrium with the moisture content of the environment [2, 3]. As water evaporates, the latent heat of the vaporized water (or heat of vaporization) is absorbed from the surrounding environment. In the absence of other mechanisms of heat transfer, a net cooling effect of the object's surface is experienced.

It is believed that high moisture bearing fibers (up to 30 wt % moisture) of polyamidobenzimidazole were used in intercontinental ballistic missile rocket motor casings to limit thermal-induced damage from laser threat [4]. Morgan et al. showed that wet composites can dissipate up to an order magnitude greater thermal energy than dry composites [5].

In the present work, the feasibility of evaporative cooling of the surface of a composite panel is numerically assessed as a means of reducing the external temperature of military aircraft. In the present formulation, we develop a simple one-dimensional model of the evaporative cooling process. We consider active evaporative cooling, where active implies that the moisture is actively fed from an internal reservoir to the outer surface of the panel by means of an active mechanical process. The governing differential equation describing the transient heat transfer is derived from the principle of energy conservation. A Galerkin weak form finite element model is used to solve the resulting nonlinear equation. We present transient surface temperature results for a variety of environmental conditions.

##### Physical Model

An illustration of the physical model is provided in Figure 1. To simplify the resulting governing equation we consider an isotropic and homogeneous flat panel or plate of dimensions  $L_p \times L_p \times L$  where  $L_p \gg L$ . Since the thickness is much smaller than the other dimensions of the plate, we will assume that the current state of the panel is a function of the thickness coordinate  $x$  and time  $t$  only. We therefore consider an open one-dimensional region  $W = (0, L)$  with closure  $\bar{W} = \{0, L\} \cup \{x, 0\} \cup \{x, L\}$

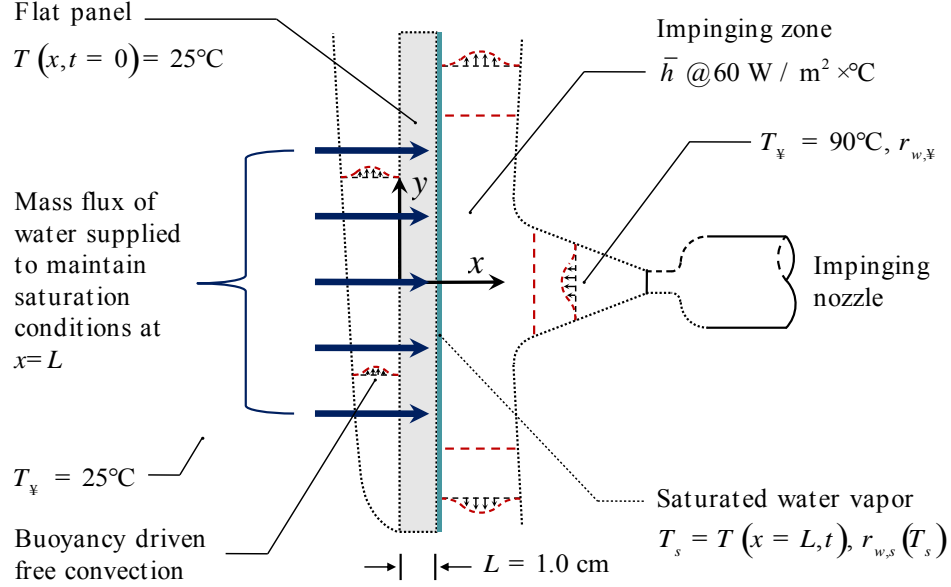


**Figure 1. The physical model.**

The plate possesses a uniform initial temperature,  $T(x, 0) = T_0$ . At  $t = 0$ , the plate is exposed on both surfaces to streams of air containing known free stream temperatures and moisture contents. At  $x = L$ , the plate is exposed to an impinging stream of air at an elevated temperature where heat transfer is induced by forced convection of the impinging fluid. At  $x = 0$ , the panel is simply exposed to stagnant air where convective heat transfer occurs by buoyancy driven fluid flow. In addition to these effects, liquid water is actively driven at a known rate through the panel where it evaporates at  $x = L$ . For the purpose of our numerical analysis, we assume that the rate of moisture flux can be mechanically controlled. We further assume that the water leaves the surface (at  $x = L$ ) by evaporation only. A more detailed mathematical description of the heat transfer process is provided in subsequent sections.

### *Derivation of Governing Heat Equation*

In this section we present a derivation of the governing equation for the coupled heat and mass transfer arising from the transport of liquid water through a composite panel. We proceed by developing the equations for a general continuum in  $\mathbb{R}^3$  and then specialize the formulation to the one-dimensional case. To this end we consider an open bounded material region  $\bar{W} \subset \mathbb{R}^3$  with boundary  $G = \partial W$  and closure  $\bar{W} = W \cup G$ . The boundary can be expressed as  $G = G_D \cup G_N$  where  $G_D \cap G_N = \emptyset$ , and  $G_D$  and  $G_N$  are the Dirichlet and Neumann boundary conditions respectively. Applying the conservation of mass and energy principles to the material points in  $W$  results in the following expressions

$$\begin{aligned} \frac{\partial r}{\partial t} + \tilde{N} \cdot (r \mathbf{v}) &= 0 \\ r \frac{De}{Dt} &= s : \mathbf{D} - \tilde{N} \cdot \mathbf{q} \end{aligned} \quad \text{in } W \quad (0, T, \mathbf{u}) \quad (1)$$

In Eq. (1)  $r$  is the density,  $\mathbf{v}$  is the velocity vector,  $e$  is the internal energy,  $s$  is the Cauchy stress tensor,  $\mathbf{D}$  is the symmetric part of the velocity gradient tensor and  $\mathbf{q}$  is the heat flux vector. In addition, the time derivative operator in Eq. (1) is the material time derivative operator and the divergence operator (i.e.,  $\tilde{\mathbf{N}} \times$ ) acts with respect to the spatial coordinates  $\mathbf{x}$ . It is convenient to express the internal energy in terms of the enthalpy  $\hat{h}$  and thermodynamic pressure  $p$  as

$$e = \hat{h} - \frac{p}{r} \quad (2)$$

In addition it is useful to decompose the Cauchy stress tensor into the sum of its hydrostatic and deviatoric parts

$$s = -p\mathbf{I} + t \quad (3)$$

where  $t$  is the deviatoric stress tensor. Using Eqs. (1), (2) and (3) allows the energy equation to be expressed as [6]

$$r \frac{D\hat{h}}{Dt} - \frac{Dp}{Dt} = t : \mathbf{D} - \tilde{\mathbf{N}} \times \mathbf{q} \quad (4)$$

For the present analysis the effects of  $p$  and  $t$  will be ignored. This leads to the following simplified energy equation

$$r \frac{\mathcal{D}\hat{h}}{\mathcal{D}t} + r \mathbf{v} \times \tilde{\mathbf{N}} \hat{h} = - \tilde{\mathbf{N}} \times \mathbf{q} \quad (5)$$

Applying the principle of mass conservation to the liquid water driven through the flat panel results in the following standard continuity equation

$$\frac{\mathcal{D}r_w}{\mathcal{D}t} + \tilde{\mathbf{N}} \times (r_w \mathbf{v}_w) = 0 \quad (6)$$

In Eq. (6),  $r_w$  is the partial density of the liquid water and  $\mathbf{v}_w$  is the velocity of the same. In the present formulation  $\mathbf{v}_w$  is taken as a known quantity. As a result it is unnecessary to solve Eq. (6).

### *Rule of Mixtures and Constitutive Relationships*

The material in this analysis is treated as a binary mixture of liquid water imbedded in a solid epoxy composite plate. Quantities associated with the bulk material such as enthalpy, thermal conductivity, velocity, etc., are expressed throughout this work using the rule of mixtures. An arbitrary quantity  $j$  associated with the bulk material is therefore approximated as

$$rj = r_w j_w + r_e j_e \quad (7)$$

where the subscripts  $e$  and  $w$  refer to the epoxy matrix and the liquid water, respectively. The quantity  $r_i$  in Eq. (7) is the partial density of a particular species. The partial density is defined as the mass of constituent  $i$  in a small representative volume of the mixture divided by the total representative volume [7]. Eq. (7) can be used to obtain the following expression

$$r \mathbf{v} \times \tilde{\mathbf{N}} \hat{h} = r_w \mathbf{v}_w \times \tilde{\mathbf{N}} \hat{h}_w \quad (8)$$

The constitutive equations employed are Fourier's law of heat conduction and the standard enthalpy-temperature relationship. For the isotropic case these equations assume the following forms

$$\mathbf{q} = -k\tilde{\mathbf{N}}T, \quad \hat{h} = c_p T \quad (9)$$

where  $k$  is the thermal conductivity and  $c_p$  is the effective specific heat of the bulk material. Using Eqs. (8) and (9) in Eq. (5) results in the following energy equation for the mixture

$$r c_p \frac{\partial T}{\partial t} + r_w c_{p,w} \mathbf{v}_w \cdot \nabla T = \tilde{\mathbf{N}} \cdot (\nabla T) \quad \text{in } W \quad (0, T) \quad (10)$$

where  $c_{p,w}$  is the specific heat of water. In Eq. (10) we have assumed that  $c_p$  is constant. For the present analysis we will be concerned with the one dimensional form of Eq. (10) which can be expressed as

$$r c_p \frac{\partial T}{\partial t} + r_w c_{p,w} v_w \frac{\partial T}{\partial x} = \frac{\partial}{\partial x} (k \frac{\partial T}{\partial x}) \quad \text{in } (0, L) \quad (0, T) \quad (11)$$

## Finite Element Model of Energy Equation

### Weak Form of Energy Equation

In this section we develop a weak form Galerkin finite element model of the energy equation given by Eq. (11). In our finite element formulation we discretize the computational domain  $\bar{W} = [0, L]$  into a set of  $NE$  non-overlapping subdomains (or elements)  $W = [x_a^e, x_b^e]$  such that  $\bar{W} = \bigcup_{e=1}^{NE} W$ . The variational or weak form problem is to find  $T \in H^1(\bar{W})$  for all test functions  $w \in H_*^1(\bar{W})$  such that

$$B(w, T) = l(w) \quad (12)$$

where the bilinear and linear forms are given as

$$\begin{aligned} B(w, T) &= \int_{x_a^e}^{x_b^e} c_p w \frac{\partial T}{\partial t} + k \frac{\partial w}{\partial x} \frac{\partial T}{\partial x} - \int_{x_a^e}^{x_b^e} (w r_w c_{p,w} v_w) T \, dx \\ l(w) &= w(x_a) Q_1 + w(x_b) Q_2 \end{aligned} \quad (13)$$

In the above expressions we have made use of the standard definition of the Sobolev space  $H^1(\bar{W}) = W^{1,2}(\bar{W})$ . The space  $H_*^1(\bar{W})$  associated with the test functions  $w$  is defined as  $H_*^1(\bar{W}) = \{w \in H^1(\bar{W}) : w = 0 \text{ on } \Gamma_T^e\}$ , where  $\Gamma_T^e$  is the element boundary where the temperature is specified.

For the sake of brevity we have dropped superscripts  $e$  from quantities in the above equations and throughout the remainder of this work. It should therefore be remembered that Eq. (12) applies to the  $e^{\text{th}}$  element of the finite element model. Assuming  $r$ ,  $c_{p,w}$  and  $v_w$  to be constant allows the bilinear form to be reduced to

$$B(w, T) = \int_{x_a}^{x_b} r c_p w \frac{\partial T}{\partial t} + k \frac{\partial w}{\partial x} \frac{\partial T}{\partial x} - r_w c_{p,w} v_w \frac{\partial w}{\partial x} T \frac{\partial}{\partial \theta} dx \quad (14)$$

The quantities  $Q_j$  are the generalized element forces which can be expressed as

$$Q_1 = - \int_{x_a}^{x_b} \frac{\partial T}{\partial x} - r_w c_{p,w} T v_w \frac{\partial}{\partial \theta} \bigg|_{\hat{u}=x_a}, \quad Q_2 = \int_{x_a}^{x_b} \frac{\partial T}{\partial x} - r_w c_{p,w} T v_w \frac{\partial}{\partial \theta} \bigg|_{\hat{u}=x_b} \quad (15)$$

### Semi-Discrete Finite Element Equations

In the present formulation we assume a space-time decoupled finite element solution. The temperature field in the weak form is therefore approximated within each finite element using the following interpolation scheme

$$T(x, t) = \sum_{j=1}^n T_j(t) y_j(x) \quad (16)$$

where  $x \in [x_a, x_b]$ . In Eq. (16),  $y_j(x)$  are the one-dimensional Lagrange interpolation functions which can be expressed as

$$y_j(x) = \prod_{k=1, k \neq j}^n \frac{x - x_k}{x_j - x_k} \quad (17)$$

where  $\xi = 2(x - x_a) / h_x - 1$  and  $h_x = x_b - x_a$ . The quantities  $x_k$  are the locations of the nodes in terms of the natural coordinate  $\xi$  [8]. We employ the standard Galerkin approach and define a set of weighting functions  $w_i(x)$  as

$$w_i(x) = y_i(x) \quad (18)$$

The semidiscrete finite element equations are obtained by inserting Eqs. (16) and (18) into Eq. (14) which results in the following element equations

$$\int_{x_a}^{x_b} \frac{\partial}{\partial t} \{ C_{ij}^e \} + \int_{x_a}^{x_b} \frac{\partial}{\partial x} \{ K_{ij}^e \} = \{ F_i^e \} \quad (19)$$

The finite element matrices appearing in Eq. (19) can be determined from the following formulas

$$\begin{aligned} C_{ij}^e &= \int_{x_a}^{x_b} r c_p y_i y_j dx \\ K_{ij}^e &= \int_{x_a}^{x_b} k \frac{dy_i}{dx} \frac{dy_j}{dx} - r_w c_{p,w} v_w \frac{dy_i}{dx} y_j \frac{\partial}{\partial \theta} dx \\ F_i^e &= y_i(x_a) Q_1 + y_i(x_b) Q_2 \end{aligned} \quad (20)$$

The standard finite element assembly operator [8] is used to construct the global set of finite element equations which assume the following general form

$$\int_{x_a}^{x_b} \frac{\partial}{\partial t} \{ C_{ij} \} + \int_{x_a}^{x_b} \frac{\partial}{\partial x} \{ K_{ij} \} = \{ F_i \} \quad (21)$$

## Fully Discretized Finite Element Equations

The fully discretized finite element equations are obtained by partitioning the time interval  $\hat{\Theta}, t_{\hat{\Omega}}$  of interest into a set of  $N$  non-overlapping subintervals such that

$$\hat{\Theta}, t_{\hat{\Omega}} = \bigcup_{s=1}^N \hat{\Theta}_s, t_{s+1} \hat{\Omega} \quad (22)$$

The solution is obtained by solving an initial value problem within each subregion  $\hat{\Theta}_s, t_{s+1} \hat{\Omega}$  where the solution is known at  $t_s$ . In seeking a solution to Eq. (21) within  $\hat{\Theta}_s, t_{s+1} \hat{\Omega}$  we replace the time derivative operator with a discrete approximation through the use of the  $a$ -family of time approximation

$$\frac{\{T\}_{s+1} - \{T\}_s}{Dt_s} = (1-a)\{T\}_s + a\{T\}_{s+1} \quad (23)$$

where  $0 \leq a \leq 1$ . Using Eq. (23) in Eq. (21) results in the following fully discretized finite element equations

$$\begin{aligned} \left( \hat{\mathcal{C}}_{\hat{\Omega}_{s+1}} + aDt_s \hat{\mathcal{K}}_{\hat{\Omega}_{s+1}} \right) \{T\}_{s+1} &= aDt_s \{F\}_{s+1} + \hat{\mathcal{C}}_{\hat{\Omega}_{s+1}} \{T\}_s \\ &- Dt_s (1-a) \hat{\mathcal{C}}_{\hat{\Omega}_{s+1}} \hat{\mathcal{C}}_{\hat{\Omega}_s}^{-1} \left( \hat{\mathcal{K}}_{\hat{\Omega}_s} \{T\}_s - \{F\}_s \right) \end{aligned} \quad (24)$$

In the present analysis we use the Crank-Nicolson scheme where  $a = 1/2$ . For linear systems this results in a temporal integration scheme that is unconditionally stable with second order accuracy with respect to the time step  $Dt_s = t_{s+1} - t_s$ . In Eq. (24) we have made no assumptions on how  $\hat{\mathcal{C}}_{\hat{\Omega}}$  evolves with time. Assuming  $\hat{\mathcal{C}}_{\hat{\Omega}}$  to be constant within a given time interval yields

$$\begin{aligned} \left( \hat{\mathcal{C}}_{\hat{\Omega}_{s+1}} + aDt_s \hat{\mathcal{K}}_{\hat{\Omega}_{s+1}} \right) \{T\}_{s+1} &= aDt_s \{F\}_{s+1} + \hat{\mathcal{C}}_{\hat{\Omega}_{s+1}} \{T\}_s \\ &- Dt_s (1-a) \left( \hat{\mathcal{K}}_{\hat{\Omega}_s} \{T\}_s - \{F\}_s \right) \end{aligned} \quad (25)$$

## Initial and Boundary Conditions

To complete the finite element formulation it is necessary to specify appropriate initial and boundary conditions. For the initial conditions, we assume that the temperature in the plate is given as

$$T(x, 0) = T_0 \quad x \in \hat{\Theta}, L \hat{\Omega} \quad (26)$$

where  $T_0$  is a real constant.

For the boundary conditions, we consider convection driven heat transfer from both top ( $x = L$ ) and bottom ( $x = 0$ ) surfaces of the flat panel. The mass flux of the water through the plate thickness is considered uniform at a given moment in time. This flux is required to be equal to the moisture evaporation flux at the top surface of the plate. The mass flux of the moisture is determined by the following formula

$$m\dot{\mathcal{L}}_w = r_w v_w = bh_m (r_{w,s} - r_{w,\infty}) \quad (27)$$

where  $h_m$  is the mass transfer coefficient and  $r_{w,s}$  is the saturated vapor density of the evaporating

fluid. The quantity  $r_{w,\forall}$  is the partial density of water vapor in the air surrounding the panel. It is important to note that this quantity is a function of the surface temperature of the plate. The parameter  $b = \frac{\dot{Q}_1}{\dot{Q}_1^{\text{max}}}$  is the ratio of the “wetted” area of the plate surface (at  $x = L$ ) to the actual surface area. When  $b = 1$  the surface is considered to be fully saturated. Using Eq. (27) allows the element stiffness matrices to be expressed as

$$K_{ij}^e = \int_{x_a}^{x_b} \int_{y_a}^{y_b} \int_{z_a}^{z_b} \frac{dy_i}{dx} \frac{dy_j}{dx} - bh_m (r_{w,s} - r_{w,\forall}) c_{p,w} \frac{dy_i}{dx} y_j \frac{\partial}{\partial x} dx \quad (28)$$

The boundary conditions for the finite element equations can be expressed in the following forms

$$Q_1^I = \dot{Q}_1 (T_{\forall} - T) + bh_m (r_{w,s} - r_{w,\forall}) c_{p,w} T \dot{u}_{\mathbf{a}=0} \quad (29)$$

$$Q_1^{NE} = \dot{Q}_1 (T_{\forall} - T) - bh_m (r_{w,s} - r_{w,\forall}) (h_{fg} + c_{p,w} T) \dot{u}_{\mathbf{a}=L} \quad (30)$$

where  $h$  is the convection heat transfer coefficient and  $T_{\forall}$  is the farfield temperature of the air. It is important to note that the values of  $h$  and  $T_{\forall}$  appearing in Eq. (29) are not necessarily the same as those appearing in Eq. (30) (see Figure 1). The boundary conditions are incorporated into the assembled finite element equations by applying the following modifications to the global stiffness matrix and force vector

$$\begin{aligned} K_{11} &= K_{11} + h - bh_m (r_{w,s} - r_{w,\forall}) c_{p,w} \\ K_{NN} &= K_{NN} + h + bh_m (r_{w,s} - r_{w,\forall}) c_{p,w} \end{aligned} \quad (31)$$

$$\begin{aligned} F_1 &= hT_{\forall} \\ F_{NN} &= hT_{\forall} - bh_m (r_{w,s} - r_{w,\forall}) h_{fg} \end{aligned} \quad (32)$$

where  $NN$  is the total number of nodes in the finite element model.

## Numerical Results and Discussion

In this section we present numerical results obtained from finite element simulations conducted using the model described in the previous section. The finite element model is implemented using the MATLAB programming language. Double precision accuracy is used for all quantities in the model. For all simulations conducted we have employed a mesh containing 25 equally spaced cubic elements ( $p = 3$ ). This amounts to 101 total degrees of freedom (or nodes) in the model. This fine mesh size is necessary in the weak form Galerkin formulation to avoid spurious oscillations in the numerical solution, due to the advection term that is present in the energy equation. The solution procedure is iterative since the saturation density of water vapor is a nonlinear function of the surface temperature. Other nonlinearities are also present in the model, as other material parameters are also functions of temperature. Curve fits of these parameters are presented in the Appendix of this report.

**Table 1. Dimensions, parameters and material properties for finite element model.**

Parameter	Description
$L = 0.01$	Panel thickness [m]
$L_p = 0.06$	Length of plate [m]
$H = 0.051$	Distance from exit of nozzle to flat plate [m]

$d_h = 0.009525$	Inner diameter of nozzle [m]
$r = 0.06$	Radial distance for averaging of h [m]
$c_{p,e} = 1,000$	Specific heat of epoxy [J/(kg K)]
$c_{p,w} = 4,181$	Specific heat of liquid water [J/(kg K)]
$\rho_e = 1,130$	Density of epoxy panel [kg/m <sup>3</sup> ]
$k_e = 0.16$	Thermal conductivity of epoxy [W/(m K)]
$V = 9.935$	Freestream velocity of air impinging against panel [m/s]
$g = 9.81$	Gravitational constant [m/s <sup>2</sup> ]

In addition to the parameters given in Table 1, we specify the freestream air temperature of the impinging jet to be given as  $T_\infty = 90^\circ\text{C}$ . For the numerical results, we perform a parametric study of the evolution of the surface temperature of the panel by varying  $b$  and the relative humidity  $f$  of the freestream impinging air. The relative humidity  $f$  is the ratio of the mass of the moisture in the air to the maximum amount of moisture the air could hold at the same temperature.

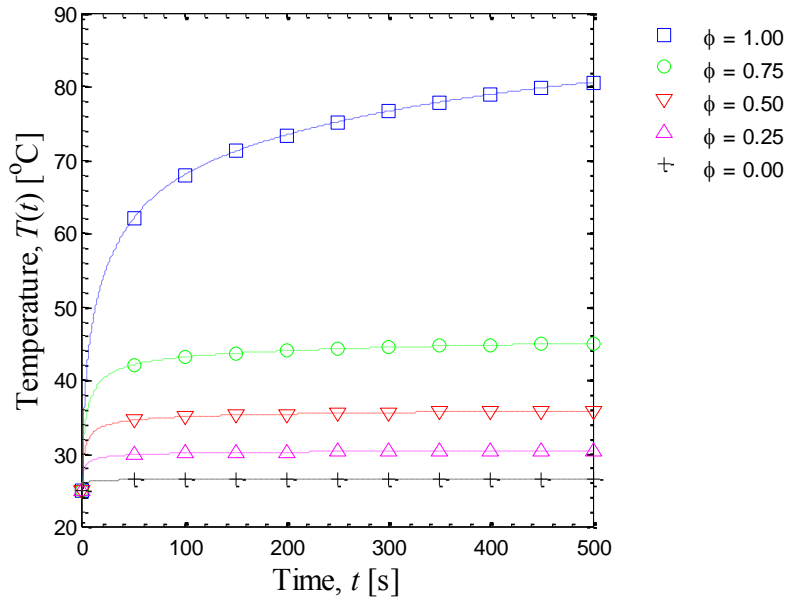


**Figure 2. Surface temperature profiles (at  $x = L$ ) of an epoxy panel exposed to an impinging jet ( $T_0 = 25^\circ\text{C}$ ,  $T_\infty = 90^\circ\text{C}$  and  $b = 1.00$ ).**

In Figures 4 through 5 we present transient surface temperature results for flat panels that each possess an initial temperature  $T_0 = 25^\circ\text{C}$ . A constant time step of  $\Delta t = 0.05$  s is employed in all cases. In each figure a different surface saturation ratio (i.e.,  $b = 0.25, 0.50, 0.75, 1.00$ ) is evaluated. Furthermore in each figure we evaluate the effect of the relative humidity  $f$  of the environment on the overall surface temperatures. As expected, the effects of evaporation play a major role in reducing the surface temperature profiles for all cases. It can be seen that under ideal circumstances, where the moisture at the surface of the panel is maintained at saturation conditions (i.e., cases where  $b = 1.00$ ), significant cooling of the surface is experienced. When the freestream air is dry, evaporation maintains the surface temperature very close to the initial temperature of the plate.

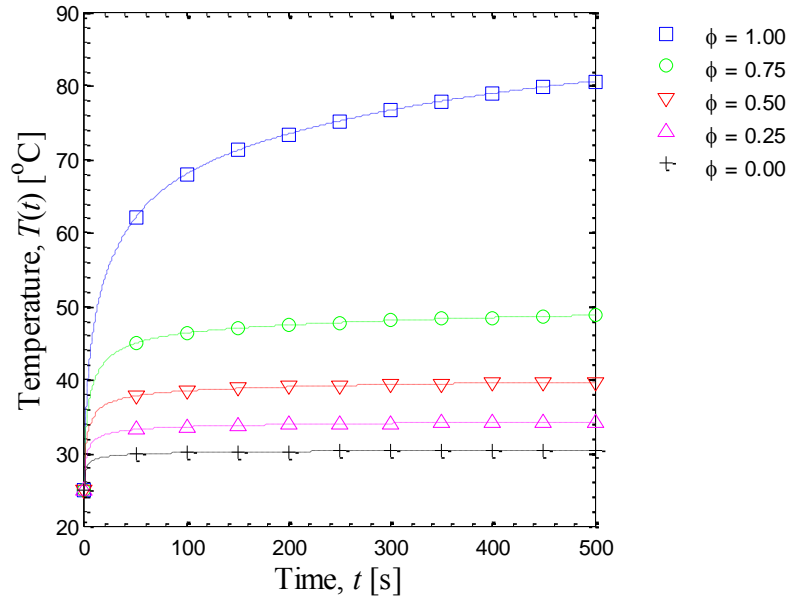


**Figure 3. Surface temperature profiles (at  $x = L$ ) of an epoxy panel exposed to an impinging jet ( $T_0 = 25^\circ\text{C}$ ,  $T_\infty = 90^\circ\text{C}$  and  $b = 0.75$ ).**

For less ideal cases (i.e., cases where  $b < 1.00$ ) the cooling effects are less pronounced, but still significant as can be seen in Figures , and . We observe a similar trend when considering the influence of the relative humidity of the external flow. More humid environments lead to less evaporation from the panel surface, and ultimately lower cooling effects.

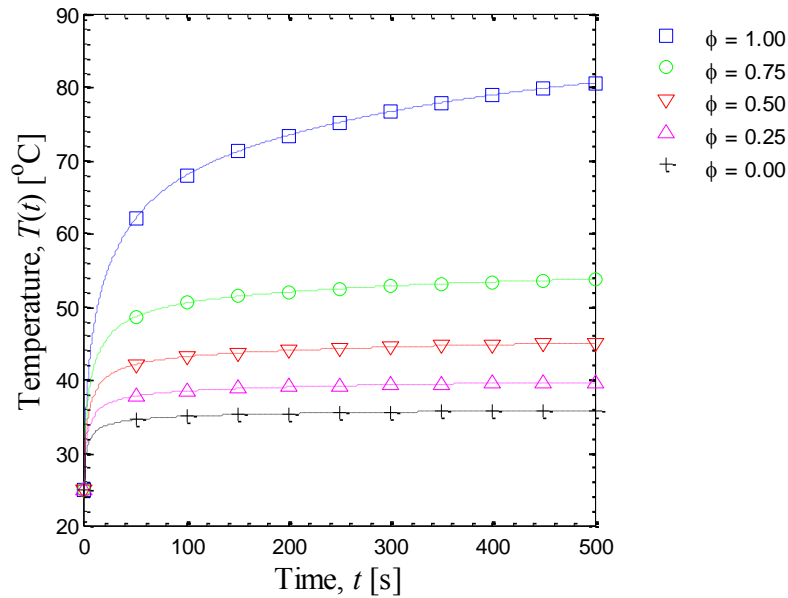


**Figure 4. Surface temperature profiles (at  $x = L$ ) of an epoxy panel exposed to an impinging jet ( $T_0 = 25^\circ\text{C}$ ,  $T_\infty = 90^\circ\text{C}$  and  $b = 0.50$ ).**

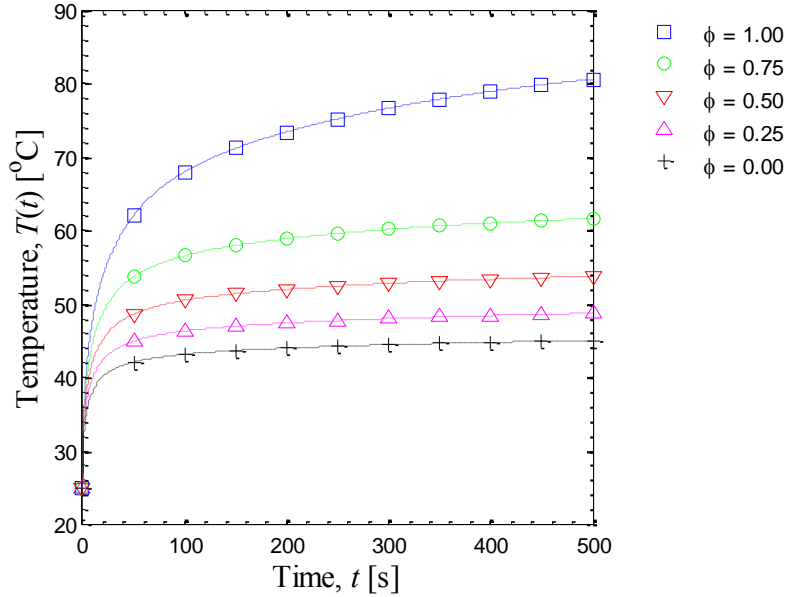


**Figure 5.** Surface temperature profiles (at  $x = L$ ) of an epoxy panel exposed to an impinging jet ( $T_0 = 25^\circ\text{C}$ ,  $T_\infty = 90^\circ\text{C}$  and  $b = 0.25$ ).

It is also important to quantify the mass of the moisture lost to the environment as a result of the evaporative cooling process. In Table 2 below we present values for the total mass (per unit area) of water lost due to evaporation during the numerical simulations as a function of the panel wetness  $b$ , and relative humidity  $f$  of the environment. Approximate average mass flux rates can be obtained by dividing the values in Table 2 by the total simulation time ( $t = 500$  s).

**Table 2.** Effect of panel wetness  $b$ , and relative environmental humidity  $f$ , on total mass (per unit area) of water vaporized in evaporation process after 500 s.

$f$	Mass of water evaporated after 500 s ( $\text{kg}/\text{m}^2$ )			
	$b = 1.00$	$b = 0.75$	$b = 0.50$	$b = 0.25$
1.000	0.000	0.000	0.000	0.000
0.750	0.490	0.434	0.359	0.246
0.500	0.631	0.571	0.490	0.359
0.250	0.716	0.655	0.571	0.434
0.000	0.776	0.716	0.631	0.490

In appraising the numerical results presented in this study, it is important to draw attention to two of the key assumptions inherent in the numerical model. First; in the present study, the convective mass transfer coefficient is determined using the well-known analogy between convective heat and mass transfer as discussed in the Appendix of this report. Actual mass transfer coefficients may deviate to some degree from the values obtained using the heat and mass transfer analogy. The second assumption is that the plate surface remains saturated and the water leaves the surface only by evaporation. In other words, we have assumed that the water is not *blown* from the surface by the impinging jet prior to evaporation.

## Conclusions

In this work we have presented a numerical model to assess the potential of active evaporative cooling as

means of reducing the external temperature of military aircraft. We introduced a simplified physical model of the phenomena consisting of a flat panel exposed to an impinging jet of hot air on one surface. Evaporative cooling was induced in the theoretical model by actively driving moisture through the panel to the outer surface. The governing heat equation for the physical model was derived from the conservation of energy principle and appropriate constitutive relationships. The equation was solved numerically using a weak form finite element formulation in conjunction with the  $a$ -family of time approximation and the Crank-Nicolson time integration scheme.

Parametric studies were conducted on a benchmark problem, where the panel wetness  $b$ , and relative environmental humidity  $f$  were varied. Surface temperature profiles were then plotted to demonstrate sensitivity of the panel's surface temperature to these parameters. The results indicate that under ideal situations, where there was low relative environmental humidity, and panel surface saturation near unity, active evaporative cooling is able to greatly reduce a panel's surface temperature. However, we can also conclude that under less ideal circumstances, the evaporation process still counters much of the heat of the impinging fluid.

## **MICROCHANNEL MODEL EXPERIMENTS**

Many problems with thermal management, signature reduction, and self-repairing materials require micro-channels in the structure. These micro-channels would allow fluids to flow through the structure to provide repair agents, collect waste heat, and to reduce surface temperature. Our experiments attempted to create a model system of microchannels.

It is hoped that various directions of fluid flow through complex microchannel networks will conduct heat reduce temperatures. Such system might dissipate enough energy with effective heat transfer through a large surface area to volume ratio. Furthermore, high thermal conductivity of carbon fiber might enhance heat conduction to the microchannel network.

### **Sample preparation**

Microchannel experiments were conducted with these materials:

- Sample material (epoxy/T-300 carbon fiber)
  - Sample size : 76.2 mm \* 76.2 mm \* 2 mm (L\*W\*H)
- Diameter of micro-channel : 100 ~ 220  $\mu\text{m}$ 
  - Sample fiber direction : 90°
- Sample preparation process (micro-channel fabrication)
  - Putting lubricated nickel chromium wires through the sheets of composite positioning fiber direction before curing
    - Applying electric current both end of wire to burn the material around the wire which makes the wire pull out smoothly.
- Pulling the wires from the composite to get micro-channel

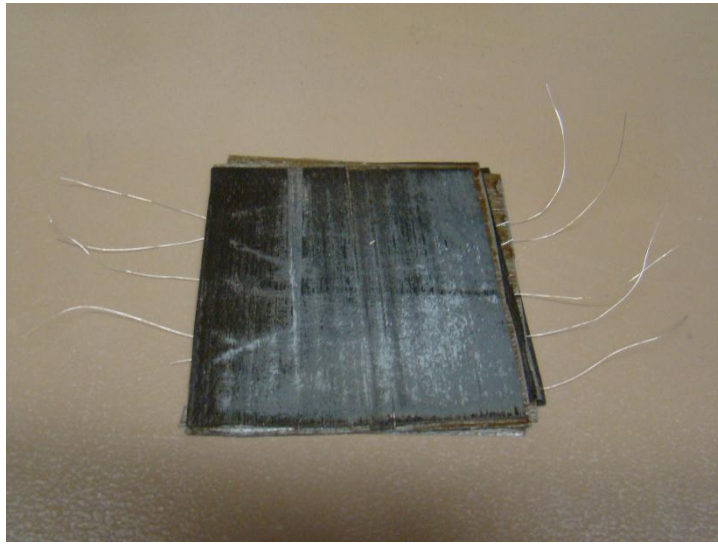


**Figure 6 (Fig 1). Nickel chromium wires in a layered composite**



**Figure 7. Variable electric current generation**

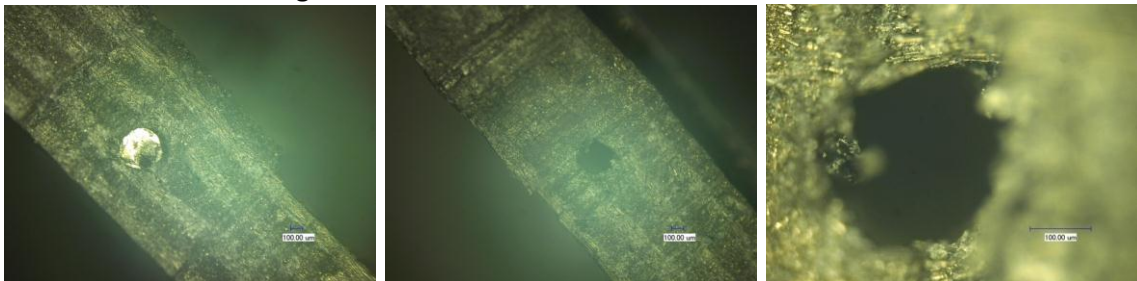


**Figure 8. Epoxy/T-300 carbon fiber with micro-channel**

Figure 6. shows a prepared sample composite material with wires after curing. To release the the wires smoothly, electric current was applied through the wires. Figure 7. shows electric current control with a variac. Finally, microchannels in the composite were fabricated as Figure 8 shows.

## Complex microchannel

First, 90° fiber angles between layers provides 90° microchannel direction changes from layer to layer. Microchannels positioned on the adjacent sheets might meet and mix fluid internally.

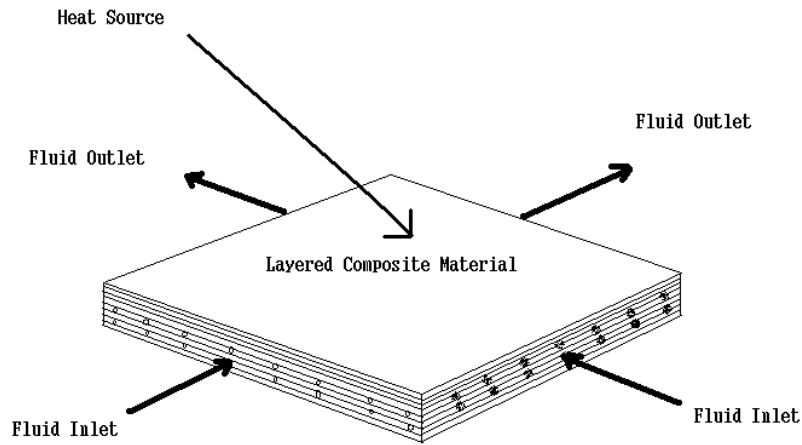


Figure 9 . Schematic diagram of 90° internal micro-channels

### Mathematical modeling of conductive heat transfer in composites

In this section, a mathematical modeling of heat transfer in composite is introduced. Composite laminate multiple fiber angles and analyzing the thermal properties of oriented fibrous composite is difficult, since fiber orientation affects thermal properties. Each lamina is transversely isotropic about its fiber axis. Consider that this case is as two-dimensional heat transfer, then  $k_{ij}$  is the thermal conductivity of any lamina [1].

$$k_{ij} = (k_a + k_t) p_i p_j + k_t \delta_{ij} \quad (1)$$

$k_a$  : axial heat conductivities

$k_t$ : transverse heat conductivities

$p_i$ : a unit vector to axial fiber direction

$\delta_{ij}$ : Kronecker delta

From the mathematical model,  $k_t$  (transverse heat conductivities) is an important property since heat source from the surface area transfer to the media transversely [2].

To find n-th layer heat conductivities,

$$\underline{k}_{xx} = \sum k^n_{xx} h^n / \sum h^n \quad (2)$$

$\bar{k}_{xx}$ : average of x direction heat conductivities

$k^n_{xx}$ : the n-th layer heat conductivity

$h^n$ : thickness

Fluid flow may be very slow and should be a laminar flow since cross sectional area of the channels is micro size. As a result of limitation of fluid velocity, conductive heat transfer dominates in the channels. Therefore, capillary action is expected, but microchannels in each layer meet neighboring microchannels in  $90^\circ$  and are expected to mix fluid actively which makes convective heat transfer increase. Furthermore, if fiber angles more complicated than  $90^\circ$ , more enhancement of heat transfer will be expected.

## Reference

- [1] Advani, S. G and C. L. Tucker III. "The Use of Tensors to Describe and Fiber Orientation in Short Fiber Composites," Journal of Rheology, 31:751 (1987)
- [2] S. J. Hwang and C. L. Tucker III, "Heat Transfer Analysis of Continuous Fiber/Thermoplastic Matrix Composites During Manufacture," Journal of Thermoplastic Composite Materials, Vol.3, Jan. p. 44 (1990)

## **PERSONNEL SUPPORTED/ASSOCIATED**

### **FACULTY**

- Dr. Terry Creasy
- Dr. J. N. Reddy

### **GRADUATE STUDENTS**

- Greg Payette
- Jaehyeuk Jeon

### **UNDERGRADUATE STUDENTS**

- Joe Schumate

## **PUBLICATIONS**

1. Y. Li, G.. S. Payette, N. Obando, J.O'Neal, J. Ju, R.J. Morgan and J.N. Reddy "Evaporative Cooling of Moisture Bearing Epoxy Composite Plate", Proceedings of SAMPE 2006 Fall Technical Conference, Dallas, TX (2006).
2. J.E. O'Neal, "Thermal Protection of High Temperature Polymer-Matrix Carbon Fiber Composites", M.S. Thesis, Texas A&M University (2006).
3. G.. Payette, "Mathematical Modeling of Evaporative Cooling of Moisture Bearing Epoxy Composite Plates", M.S. Thesis, Texas A&M University (2006).
4. R. J. Morgan, T. Creasy, Y. Li, J. Ju, F. Tschen, N. Obando, O. Ewumi and J.E. Lincoln, "Composite Thermal-Induced Degradation Mechanisms and Protection for Future Aerospace Vehicles", Proceedings of 27<sup>th</sup> High Temple Workshop, Sedona, AZ, February, 2007.
5. J. Ju, R.J. Morgan, Terry S. Creasy and J.N. Reddy, "Multifunctional Evaporative Surface Cooling for Minimizing Infrared (IR) Detection", ASME International Mechanical Engineering Congress and Exposition, November 11-15, 2007, Seattle, Washington (Accepted).
6. J. Ju, R.J. Morgan, Terry S. Creasy and J.N. Reddy, "Evaporative Cooling of Moisture Bearing Composites for Hypersonic Vehicles", Proceedings of 4<sup>th</sup> U.S. - Korea Science and Engineering Conference, August 9-12, 2007, Washington D.C. (Accepted).

## APPENDIX

### A. CONVECTIVE HEAT TRANSFER COEFFICIENTS

The convective heat transfer coefficients  $h$  are determined from a combination of analytical and empirical formulas that are readily available in the literature [2,7,9]. In the case of a single round nozzle discharging fluid against a flat surface (i.e., a single impinging jet), the Reynolds and average Nusselt numbers are defined as [7]

$$Re \circ \frac{Vd_h}{k_a} \quad (\text{A.1})$$

$$\overline{Nu} \circ \frac{\overline{h}d_h}{k_a} \quad (\text{A.2})$$

where  $d_h$  is the inner diameter of the nozzle from which the gas stream is flowing,  $k_a$  is the thermal conductivity of the air and  $V$  is the air velocity. The following expression is obtained from the literature for approximating the average convection heat transfer coefficient  $\overline{h}$  [7]

$$\overline{h} = \frac{2k_a Re^{1/2} Pr^{0.42} (1 - 1.1d_h / r)(1 + 0.005 Re^{0.55})^{1/2}}{r \frac{c}{\rho} + 0.1(H / d_h - 6)d_h / r \frac{c}{\rho}} \quad (\text{A.3})$$

where the Prandtl number is defined in general as

$$Pr \circ \frac{v_a r_a c_{p,a}}{k_a} \quad (\text{A.4})$$

In Eq. (A.4), the quantities  $v_a$ ,  $r_a$  and  $c_{p,a}$  are the kinematic viscosity, density and specific heat of air. Eq. (A.3) is used to estimate the average convection heat transfer coefficient  $\overline{h}$  in the vicinity of the stagnation point of the flow. The quantity  $r$  is the radial distance from the stagnation point to an arbitrary distance on the surface of the plate over which  $\overline{h}$  is averaged. The quantity  $H$  is the distance from the exit plane of the nozzle to the surface of the flat plate.

It is also necessary to determine the average convective heat transfer coefficient for the bottom side of the plate ( $x = 0$ ) where convection occurs due to buoyancy driven flow conditions. For free convection (i.e., buoyancy driven flows) the averaged Nusselt number is given as [10]

$$\overline{Nu} \circ \frac{\overline{h}L_p}{k_a} \quad (\text{A.5})$$

In addition, the Rayleigh number,  $Ra_L$ , is defined as [10]

$$Ra_L = \frac{g r_a c_{p,a} |T_s - T_\infty| L_p^3}{v_a k_a T_f} \quad (\text{A.6})$$

where  $g$  is the gravitational constant. The averaged Nusselt number is given as [10]

$$\overline{Nu} = 0.68 + \frac{0.670 Ra_L^{1/4}}{\frac{c}{\rho} + (0.492 / Pr)^{9/16} \frac{c}{\rho}} \quad Ra_L < 10^9 \quad (\text{A.7})$$

The average convective heat transfer coefficient  $\bar{h}$  for free convection may therefore be determined from Eqs. (A.4) through (A.7).

## B. CONVECTIVE MASS TRANSFER COEFFICIENTS

It is also necessary to determine the convective mass transfer coefficient  $h_m$ . To do so it is important to introduce some non-dimensional parameters. The Schmidt number  $Sc$  is defined as [7]

$$Sc = \frac{\nu_a}{D_a} \quad (B.1)$$

For parallel flow over a flat plate the average Sherwood number is given as [7]

$$\overline{Sh} = \frac{\overline{h_m} L_p}{D_a} \quad (B.2)$$

where the quantity  $D_a$  is the diffusivity of water vapor in air. In the case of a single impinging jet, the average Sherwood number is expressed as [7]

$$\overline{Sh} = \frac{\overline{h_m} d_h}{D_a} \quad (B.3)$$

There are strong analogies between heat and mass transfer. This often leads to a similarity between the convective heat and mass transfer coefficients. This correspondence is of the form [2,7,9]

$$\frac{Nu}{Pr^n} = \frac{Sh}{Sc^n} \quad (B.4)$$

where  $Nu$  and  $Sh$  may be local or averaged quantities. If the heat transfer coefficient is known, the mass transfer coefficient may be determined from Eq. (B.4). The above analogy holds for low rates of mass transfer [2,9]. Eq. (B.4) can be used to obtain the following expression for the convective mass transfer coefficients

$$h_m = \frac{h}{r_a c_{p,a} \frac{k_a}{r_a c_{p,a} D_a} \theta^{1-n}} \quad (B.5)$$

For parallel flow over a flat plate it has been shown that  $n = 1/3$  [9]. For the case of flow from impinging jets it has been suggested that  $n = 0.42$  [9].

## C. MATERIAL PROPERTIES

Many of the material properties and coefficients used in this work are not constant. Some vary significantly with temperature and/or pressure. In this work variables are assumed to be a function of temperature only. The following are curve fits of some of the published properties of air [7] at atmospheric pressure

$$r_a = - 7.9282 \cdot 10^{-14} T_f^5 + 9.5330 \cdot 10^{-11} T_f^4 - 5.0164 \cdot 10^{-8} \cdot T_f^3 + 1.68472 \cdot 10^{-5} T_f^2 - 0.0047 T_f + 1.2770 \quad (\text{C.1})$$

$$c_{p,a} = - 8.8889 \cdot 10^{-14} T_f^6 + 9.9528 \cdot 10^{-11} T_f^5 - 4.2892 \cdot 10^{-8} T_f^4 + 8.2319 \cdot 10^{-6} T_f^3 - 0.0002 T_f^2 + 0.0153 T_f + 1006.5729 \quad (\text{C.2})$$

$$v_a = - 4.1026 \cdot 10^{-19} T_f^5 + 3.1179 \cdot 10^{-16} T_f^4 - 1.3269 \cdot 10^{-13} T_f^3 + 1.2036 \cdot 10^{-10} T_f^2 + 8.8727 \cdot 10^{-8} T_f + 1.3414 \cdot 10^{-5} \quad (\text{C.3})$$

$$k_a = 1.8461 \cdot 10^{-15} T_f^5 - 1.4637 \cdot 10^{-12} T_f^4 + 3.6606 \cdot 10^{-10} T_f^3 - 5.7872 \cdot 10^{-18} T_f^2 + 7.93825 \cdot 10^{-5} T_f + 0.0242 \quad (\text{C.4})$$

$$Pr = 1.3778 \cdot 10^{-15} T_f^6 - 1.2822 \cdot 10^{-12} T_f^5 + 4.3350 \cdot 10^{-10} T_f^4 - 6.31081 \cdot 10^{-8} T_f^3 + 3.8276 \cdot 10^{-6} T_f^2 - 2.3383 \cdot 10^{-4} T_f + 0.7117 \quad (\text{C.5})$$

Eqs. (C.1) through (C.5) are valid between -23C and 300C. The film temperature  $T_f = \frac{1}{2}(T + T_{\infty})$  possesses units of Celsius. The diffusion coefficient of water vapor in air is taken from the literature [11] as

$$D_a = 1.87 \cdot 10^{-10} (T_f + 273)^{2.072} \quad (\text{C.6})$$

The latent heat of vaporization of water  $h_{fg}$  and the saturation density of water vapor  $r_{w,s}$  are given by the following curve fits of the published data [12]

$$h_{fg} = 2.750 \cdot 10^{-10} T_f^6 - 2.9275 \cdot 10^{-7} T_f^5 + 7.67128 \cdot 10^{-5} T_f^4 - 0.0211 T_f^3 + 0.90009 T_f^2 - 22,372.6057 T_f + 2,501,365.4834 \quad (\text{C.7})$$

$$r_{w,s} = 1.6978 \cdot 10^{-14} T_f^6 - 1.8031 \cdot 10^{-12} T_f^5 + 4.3235 \cdot 10^{-9} \cdot T_f^4 - 4.5824 \cdot 10^{-8} \cdot T_f^3 + 1.8577 \cdot 10^{-5} T_f^2 + 2.1331 \cdot 10^{-4} T_f + 5.1586 \cdot 10^{-3} \quad (\text{C.8})$$

## REFERENCES

- [1] Li, Y., Morgan, R.J., and Tchen, F. Structure-Property Relations of Phenylethynyl Terminated Imide Oligomers In: Proceedings of 50th ISSE, SAMPE 2005; May 1-5, Long Beach, CA.
- [2] Bird, B. R., Stewart, W. E. and Lightfoot, E. N. Transport Phenomena. John Wiley & Sons, Inc., New York, 1960.
- [3] Panton, R. L. Incompressible Flow, (2nd Edition). John Wiley & Sons, Inc., New York, 1996.
- [4] Morgan, R. J., Pruneda C. O. and Pruneda J. Characterization of Fiber S, Lawrence Livermore National Laboratory, Internal Report, 1984.
- [5] Morgan, R. J., Kong, F. M. and Lepper, J. K. Journal of Composite Materials 1988; **22**(11):1026-1044.
- [6] Kuo, K. K. Principles of Combustion, (2nd Edition). John Wiley & Sons, Inc., New York, 2005.
- [7] Incropera, F. P., DeWitt, D. P. Fundamentals of Heat and Mass Transfer, (5th Edition). John Wiley & Sons, Inc., New York, 2002.
- [8] Reddy, J. N. An Introduction to the Finite Element Method (3rd Edition). McGraw Hill, New York, 2006.
- [9] Lienhard, J. H. IV. and Lienhard, J. H. V. A Heat Transfer Textbook (3rd Edition). Phlogiston Press, Cambridge, MA, 2005.
- [10] Welty, J. R. Wicks, C. E. and Wilson, R. E. Fundamentals of Momentum, Heat and Mass Transfer. John Wiley & Sons, Inc., New York, 1969.
- [11] Mills, A.F. Mass Transfer (2nd Edition). Prentice Hall, Inc., Upper Saddle River, NJ, 2001.
- [12] Cengel, Y.A. and Boles, M.A. Thermodynamics: An Engineering Approach (4th Edition). McGraw-Hill, New York., 2002.